

# JOURNAL OF GLACIOLOGY



**CAMBRIDGE**  
UNIVERSITY PRESS

THIS MANUSCRIPT HAS BEEN SUBMITTED TO THE JOURNAL OF GLACIOLOGY AND HAS NOT BEEN PEER-REVIEWED.

## Future projections for the Antarctic ice sheet until the year 2300 with a climate-index method

Journal:	<i>Journal of Glaciology</i>
Manuscript ID	JOG-22-0052.R1
Manuscript Type:	Article
Date Submitted by the Author:	08-Mar-2023
Complete List of Authors:	Greve, Ralf; Hokkaido University, Institute of Low Temperature Science; Hokkaido University, Arctic Research Center Chambers, Christopher; Hokkaido University, Institute of Low Temperature Science Obase, Takashi; The University of Tokyo, Atmosphere and Ocean Research Institute Saito, Fuyuki; JAMSTEC, RIGC Chan, Wing-Le; The University of Tokyo, Atmosphere and Ocean Research Institute Abe-Ouchi, Ayako; The University of Tokyo, Atmosphere and Ocean Research Institute
Keywords:	Antarctic glaciology, Climate change, Ice and climate, Ice-sheet modelling
Abstract:	As part of the Coupled Model Intercomparison Project Phase 6 (CMIP6), the Ice Sheet Model Intercomparison Project for CMIP6 (ISMIP6) was devised to assess the likely sea-level-rise contribution from the Earth's

ice sheets. Here, we construct an ensemble of climate forcings for Antarctica until the year 2300 based on original ISMIP6 forcings until 2100, combined with climate indices from simulations with the MIROC4m climate model until 2300. We then use these forcings to run simulations for the Antarctic ice sheet with the SICOPOLIS model. For the unabated warming pathway RCP8.5/SSP5-8.5, the ice sheet suffers a severe mass loss, amounting to  $\sim 1.5$  m SLE (sea-level equivalent) for the fourteen-experiment mean, and  $\sim 3.3$  m SLE for the most sensitive experiment. Most of this loss originates from West Antarctica. For the reduced emissions pathway RCP2.6/SSP1-2.6, the loss is limited to a three-experiment mean of  $\sim 0.16$  m SLE. The means are approximately two times larger than what was found in a previous study (Chambers and others, 2022, doi: 10.1017/jog.2021.124) that assumed a sustained late-21st-century climate beyond 2100, demonstrating the importance of continuously projected Antarctic climate change in the 22nd and 23th centuries.

SCHOLARONE™  
Manuscripts

# Future projections for the Antarctic ice sheet until the year 2300 with a climate-index method

Ralf GREVE<sup>1,2</sup>, Christopher CHAMBERS<sup>1</sup>, Takashi OBASE<sup>3</sup>, Fuyuki SAITO<sup>4</sup>,  
Wing-Le CHAN<sup>3,4</sup>, Ayako ABE-OUCHI<sup>3</sup>

<sup>1</sup>*Institute of Low Temperature Science, Hokkaido University, Sapporo, Japan*

<sup>2</sup>*Arctic Research Center, Hokkaido University, Sapporo, Japan*

<sup>3</sup>*Atmosphere and Ocean Research Institute, University of Tokyo, Kashiwa, Japan*

<sup>4</sup>*Japan Agency for Marine-Earth Science and Technology, Yokohama, Japan*

*Correspondence: Ralf Greve <greve@lowtem.hokudai.ac.jp>*

**ABSTRACT.** As part of the Coupled Model Intercomparison Project Phase 6 (CMIP6), the Ice Sheet Model Intercomparison Project for CMIP6 (ISMIP6) was devised to assess the likely sea-level-rise contribution from the Earth's ice sheets. Here, we construct an ensemble of climate forcings for Antarctica until the year 2300 based on original ISMIP6 forcings until 2100, combined with climate indices from simulations with the MIROC4m climate model until 2300. We then use these forcings to run simulations for the Antarctic ice sheet with the SICOPOLIS model. For the unabated warming pathway RCP8.5/SSP5-8.5, the ice sheet suffers a severe mass loss, amounting to  $\sim 1.5$  m SLE (sea-level equivalent) for the fourteen-experiment mean, and  $\sim 3.3$  m SLE for the most sensitive experiment. Most of this loss originates from West Antarctica. For the reduced emissions pathway RCP2.6/SSP1-2.6, the loss is limited to a three-experiment mean of  $\sim 0.16$  m SLE. The means are approximately two times larger than what was found in a previous study (Chambers and others, 2022, doi: 10.1017/jog.2021.124) that assumed a sustained late-21st-century climate beyond 2100, demonstrating the importance of continuously projected Antarctic climate change in the 22nd and 23th centuries.

## 1 INTRODUCTION

The ice sheets of Antarctica and Greenland are the largest potential contributors to future sea-level rise caused by global warming because of their enormous volumes. These amount to  $57.9 \pm 0.9$  m SLE (sea-level equivalent) for the Antarctic ice sheet (AIS) (Morlighem and others, 2020) and  $7.42 \pm 0.05$  m SLE for the Greenland ice sheet (GrIS) (Morlighem and others, 2017). Observations revealed that both ice sheets have been losing substantial amounts of mass since the 1990s. For the period 2012–2017, The IMBIE Team (2018) reported a mass loss of  $219 \pm 43$  Gt a<sup>-1</sup> for the AIS, most of which originates from the West Antarctic ice sheet (WAIS), and The IMBIE Team (2020) reported a loss of  $244 \pm 28$  Gt a<sup>-1</sup> for the GrIS (IMBIE: Ice sheet Mass Balance Inter-comparison Exercise). Therefore, the recent absolute losses are of similar size (likely somewhat larger for the GrIS), whereas the relative loss (compared to the total mass) is approximately 10 times smaller for the AIS compared to the GrIS. For both ice sheets, changes in the surface mass balance (SMB) as well as dynamic changes contribute to the mass loss.

A particular threat for the WAIS is that it may undergo a rapid, catastrophic disintegration through a process known as marine-ice-sheet instability (MISI) (e.g., Weertman, 1974; Mercer, 1978; Thomas and Bentley, 1978; Schoof, 2007). In contrast to the East Antarctic ice sheet (EAIS), large parts of the WAIS are grounded on a bed which is below sea level and sloping downward inland. Therefore, an initial retreat of the grounding line causes the ice sheet to be thicker at its new location, which may increase discharge and thus mass loss, so that the grounding line retreats even further in a runaway fashion. There is paleoclimatic evidence that the WAIS collapsed during past warm periods (Pollard and DeConto, 2009; Alley and others, 2015; Dutton and others, 2015; Gasson and others, 2016; Turney and others, 2020). Recent observations indicate that a new instability may already be in its initial phase (e.g., Joughin and others, 2014; Rignot and others, 2014; The IMBIE Team, 2018).

To estimate the future contribution of the AIS and GrIS to sea-level rise until the end of the 21st century, the Ice Sheet Model Intercomparison Project for CMIP6 (ISMIP6) was devised (Nowicki and others, 2016, 2020). It is part of the Coupled Model Intercomparison Project Phase 6 (CMIP6), a major international climate modelling initiative (Eyring and others, 2016) with the main goal to provide input for the recently published Sixth Assessment Report (AR6) of the Intergovernmental Panel on Climate Change (IPCC) (IPCC, 2021). For the AIS, when forced by output from CMIP5 global climate models (GCMs), a mass loss in the range of  $-7.8$  to  $30.0$  cm SLE was found under the unabated warming pathway RCP8.5

56 [RCP: Representative Concentration Pathway] (Seroussi and others, 2020). The limited number of results  
57 for the reduced emissions pathway RCP2.6 fall within this range, and so do the results obtained with  
58 CMIP6 climate forcings (Payne and others, 2021). This rather unclear picture for the AIS is a consequence  
59 of the counteracting effects of mass loss due to ocean warming and mass gain from increased snowfall. The  
60 main findings for the GrIS, when forced by output from CMIP5 GCMs, were contributions of  $90 \pm 50$  and  
61  $32 \pm 17$  mm SLE for RCP8.5 and RCP2.6, respectively (Goelzer and others, 2020). The CMIP6 GCMs tend  
62 to feature a warmer atmosphere, which results in higher mass loss due to increased surface melt (Payne  
63 and others, 2021).

64 The full suite of ISMIP6 experiments with both CMIP5 and CMIP6 forcings was carried out with  
65 the ice-sheet model SICOPOLIS (“SIMulation COde for POLythermal Ice Sheets”, [www.sicopolis.net](http://www.sicopolis.net)), as  
66 documented in detail by Greve and others (2020a,b). Chambers and others (2022) extended the ISMIP6  
67 simulations for the AIS with SICOPOLIS until the year 3000, assuming a sustained late-21st-century  
68 climate beyond 2100 (atmospheric forcing randomly sampled from the 10-year interval 2091–2100, oceanic  
69 forcing kept fixed at 2100 values). Compared to the uncertain response projected over the ISMIP6 period,  
70 a radically different picture emerges, demonstrating that the consequences of the high-emissions scenario  
71 RCP8.5/SSP5-8.5 [SSP: Shared Socioeconomic Pathway] are much greater than the 100-year response in  
72 the long term even if no further climate trend is applied beyond 2100. A similar study for the GrIS was  
73 conducted by Greve and Chambers (2022).

74 Other studies on the response of the AIS to longer-term climate change have also been conducted.  
75 Schaeffer and others (2012) and Levermann and others (2013) used statistical relationships between past  
76 temperatures and global sea levels to predict future sea-level change from all sources, including the ice  
77 sheets. Golledge and others (2015) used the Parallel Ice-Sheet Model (PISM) to demonstrate that at-  
78 mospheric warming in excess of 1.5 to 2°C above present, triggers ice-shelf collapse and a centennial to  
79 millennial-scale response by the AIS. They simulated a contribution to sea-level rise from Antarctica under  
80 higher emission scenarios of 0.6 to 3 m by the year 2300. Similarly, Garbe and others (2020) found that at  
81 greater than 2°C of global average warming, the WAIS is committed to long-term partial collapse. They  
82 also found distinct regimes in the rates of sea-level rise per degree, with a doubling in the rate if warming  
83 becomes greater than 2°C. Bulthuis and others (2019) carried out AIS projections until 3000 based on  
84 spatially uniform temperature-anomaly time-series and a combination of simulations with the fast Element-  
85 ary Thermomechanical Ice Sheet (f.ETISh) model, an emulator, probabilistic methods and uncertainty

86 quantification. They found that, irrespective of parametric uncertainty, the WAIS remains stable under  
87 RCP2.6, while RCP8.5 triggers its collapse under almost all investigated cases. In the ISMIP6-endorsed  
88 Antarctic BUttrressing Model Intercomparison Project (ABUMIP; Sun and others, 2020), the response of  
89 the AIS to sudden and sustained loss of ice shelves was simulated by an ensemble of 15 ice-sheet models.  
90 It was found that this leads to a multi-metre (1–12 m) contribution to sea-level rise over the 500-year-long  
91 simulations. Lowry and others (2021) used statistical emulation based on simulations with PISM to inves-  
92 tigate the evolution of the AIS until 2300 under RCP8.5 and RCP2.6, assuming no further climate change  
93 beyond 2100 (similar to Chambers and others, 2022). The contribution to sea-level rise was found to be  
94 indistinguishable between the two pathways in the 21st century, while multi-metre differences occur in sub-  
95 sequent centuries. DeConto and others (2021) used their observationally calibrated ice-sheet–shelf model  
96 for simulations until 2100 and extended until 2300. Their results demonstrate the possibility that rapid  
97 and unstoppable sea-level rise from the AIS will be triggered if Paris Agreement targets (limiting global  
98 mean warming in the 21st century to less than 2°C above pre-industrial levels) are exceeded. Lipscomb  
99 and others (2021) used the Community Ice Sheet Model (CISM) to investigate the response of the AIS to  
100 ISMIP6 ocean thermal forcings only, extended to 2500. They found long-term retreat of the WAIS and  
101 showed that the Amundsen sector exhibits threshold behaviour with modest retreat or complete collapse,  
102 depending on parameter settings in the melt scheme, ocean forcing, and basal friction law. Complete  
103 collapse of the WAIS occurred under some combinations of low basal friction and high thermal forcing  
104 anomalies. Van Breedam and others (2020) projected the response of the AIS and GrIS 10,000 years into  
105 the future with the Earth system model of intermediate complexity LOVECLIMv1.3 (LOVECLIM: LOch-  
106 Vecode–Ecbilt–CLio–agIsm Model), including the ice-sheet model AGISM (Antarctic and Greenland Ice  
107 Sheet Model), forced by the extended concentration pathways ECP2.6, 4.5, 6.0 and 8.5 until 2300 and zero  
108 emissions thereafter. For the AIS, they report mass losses ranging from about 1.6 m SLE for the lowest  
109 forcing scenario until up to 27 m SLE for the higher-forcing scenarios.

110 In the present study, we follow an approach similar to Chambers and others (2022), extending the  
111 ISMIP6-Antarctica simulations further into the future. However, we drop the assumption of a sustained  
112 climate with no warming or cooling trend beyond 2100. Instead, to account for greenhouse-gas emissions  
113 pathways and climate inertia after the 21st century, we construct extensions of all ISMIP6-Antarctica  
114 climate forcings until 2300 by a climate-index method explained in Sect. 2. The set-up of SICOPOLIS and  
115 the 18 model experiments (1 control, 14 RCP8.5/SSP5-8.5, 3 RCP2.6/SSP1-2.6) are explained in Sect. 3.

116 The results are described in Sect. 4, and a discussion and conclusion is provided in Sect. 5.

## 117 2 CLIMATE FORCING

118 We construct an ensemble of climate forcings for Antarctica for the period 2015–2300 by combining re-  
 119 sults from MIROC4m (MIROC: Model for Interdisciplinary Research On Climate) RCP8.5 and RCP4.5  
 120 simulations for 1995–2300 (partially published in Bakker and others, 2016) with the ensemble of ISMIP6  
 121 forcings for 2015–2100 (Nowicki and others, 2020; Seroussi and others, 2020; Payne and others, 2021). To  
 122 do so, we derive a set of atmospheric and oceanic climate indices from the MIROC4m simulations such that  
 123 1995–2014 averages of the considered fields are mapped to zero and 2091–2100 averages to unity (Sect. 2.1).  
 124 We then use the climate indices to extrapolate the ensemble of ISMIP6 forcings to the period 2101–2300  
 125 (Sect. 2.2). Together with the original ISMIP6 forcings, this method provides smooth climate forcings for  
 126 the entire period 2015–2300. Beyond the needs of this study, the method is applicable in general to extend  
 127 climate forcings of limited duration.

### 128 2.1 Climate indices

129 We define five atmospheric and one oceanic climate indices. For the atmosphere, the considered fields  
 130 are the mean-annual surface temperature (ST), summer (December–January–February, DJF) surface  
 131 temperature (ST\_DJF), precipitation (prec), evaporation (evap) and surface runoff (roff). ST and SMB =  
 132 prec – evap – roff define the atmospheric forcing, while ST\_DJF is required for the parameterization of  
 133 ice-shelf collapse (see the last part of Sect. 2.2).

All fields are spatially averaged over the AIS land grid (excluding the ice shelves because they are not  
 contained in the MIROC4m set-up), and then mapped linearly on a dimensionless scale such that

$$\begin{aligned} c_{xx}(\text{1995–2014 average}) &= 0, \\ c_{xx}(\text{2091–2100 average}) &= 1, \end{aligned} \tag{1}$$

134 where  $xx \in \{\text{ST}, \text{ST\_DJF}, \text{prec}, \text{evap}, \text{roff}\}$ . This yields the five atmospheric climate indices  $c_{\text{ST}}$ ,  $c_{\text{ST\_DJF}}$ ,  
 135  $c_{\text{prec}}$ ,  $c_{\text{evap}}$  and  $c_{\text{roff}}$ .

136 For the ocean, we use the average temperature south of 62.5°S and between 200 and 800 metres depth.  
 137 This domain encompasses the Southern Ocean surrounding the ice-shelf cavities and a range of typical  
 138 ice-shelf drafts where basal melting takes place. Non-dimensionalization with the same pinning points as

139 defined by Eq. (1) ( $xx = oc$ ) provides the oceanic climate index  $c_{oc}$ .

Since the MIROC4m results are available for RCP8.5 and RCP4.5, the above method provides climate indices for these two pathways. However, ISMIP6 covers RCP8.5 and RCP2.6, so that we also require the climate indices for RCP2.6. To obtain these, we extrapolate the atmospheric and oceanic indices for RCP8.5 and RCP4.5, assuming linear relations between the indices and the radiative forcing of the RCP scenarios:

$$c_{xx}^{\text{RCP2.6}} = c_{xx}^{\text{RCP4.5}} - \frac{4.5 - 2.6}{8.5 - 4.5} \times (c_{xx}^{\text{RCP8.5}} - c_{xx}^{\text{RCP4.5}}). \quad (2)$$

140 The resulting climate indices are shown in Figure 1. For RCP8.5, the change of all six variables during  
 141 the 22nd and 23rd century goes well beyond late-21st-century levels. The five atmospheric indices evolve  
 142 into a certain saturation towards the end of the period, whereas the oceanic index increases steadily. This  
 143 is due to the larger inertia of the ocean compared to the atmosphere. For RCP2.6, the atmospheric indices  
 144 largely fall below their late-21st-century levels, indicating a partial recovery of the climate change. By  
 145 contrast, the oceanic index does not show such a recovery and keeps on increasing (albeit at a decreasing  
 146 rate), which again results from the larger oceanic inertia.

## 147 2.2 Scaling of the ISMIP forcings

148 The ISMIP6 forcings for the AIS consist of anomalies for the surface temperature  
 149  $[\Delta\text{ST}(x, y, t)]$  and the surface mass balance  $[\Delta\text{SMB}(x, y, t)]$  relative to 1995–2014, and absolute values  
 150 for the oceanic thermal forcing  $[\text{TF}(x, y, z, t)]$ , all for the period 2015–2100. These were derived from a  
 151 systematic sampling of CMIP5 GCMs that reflects their spread in future projections (Barthel and others,  
 152 2020), while CMIP6 GCMs were added mostly on the basis of availability (Payne and others, 2021). The at-  
 153 mospheric forcings  $\Delta\text{ST}$  and  $\Delta\text{SMB}$  enter the ice-sheet simulations directly as upper boundary conditions.  
 154 By contrast, TF is used to compute sub-ice-shelf melt rates via a non-local quadratic parameterization  
 155 (“ISMIP6 standard approach”) calibrated by observations (Jourdain and others, 2020).

To extend the ISMIP6 forcings until 2300, the oceanic thermal forcing is converted to an anomaly as well by subtracting the 1995–2014 mean:

$$\Delta\text{TF}(x, y, z, t) = \text{TF}(x, y, z, t) - \text{TF}_{1995-2014}(x, y, z), \quad t \leq 2100 \text{ CE}. \quad (3)$$



We then scale the anomalies by using the MIROC4m-derived climate indices as follows:

$$\begin{aligned}
 \Delta\text{ST}(x, y, t) &= c_{\text{ST}}(t) \times \Delta\text{ST}_{2091-2100}(x, y), \\
 \Delta\text{prec}(x, y, t) &= c_{\text{prec}}(t) \times \Delta\text{prec}_{2091-2100}(x, y), \\
 \Delta\text{evap}(x, y, t) &= c_{\text{evap}}(t) \times \Delta\text{evap}_{2091-2100}(x, y), \quad t > 2100 \text{ CE}, \\
 \Delta\text{roff}(x, y, t) &= c_{\text{roff}}(t) \times \Delta\text{roff}_{2091-2100}(x, y), \\
 \Delta\text{TF}(x, y, z, t) &= c_{\text{oc}}(t) \times \Delta\text{TF}_{2091-2100}(x, y, z),
 \end{aligned} \tag{4}$$

where  $\Delta\text{prec}$ ,  $\Delta\text{evap}$  and  $\Delta\text{roff}$  are the anomalies of precipitation, evaporation and runoff, respectively, and the subscripts “2091–2100” denote the mean values over this decade. The anomaly  $\Delta\text{SMB}$  results from

$$\Delta\text{SMB}(x, y, t) = \Delta\text{prec}(x, y, t) - \Delta\text{evap}(x, y, t) - \Delta\text{roff}(x, y, t), \quad t > 2100 \text{ CE}, \tag{5}$$

and  $\Delta\text{TF}$  is converted back to absolute values:

$$\text{TF}(x, y, z, t) = \text{TF}_{1995-2014}(x, y, z) + \Delta\text{TF}(x, y, z, t), \quad t > 2100 \text{ CE}. \tag{6}$$

156 Thus, this method provides extended ISMIP6 forcings for the AIS [ $\Delta\text{ST}(x, y, t)$ ,  
 157  $\Delta\text{SMB}(x, y, t)$ ,  $\text{TF}(x, y, z, t)$ ] until the year 2300. Table 1 shows the magnitude of the atmospheric and  
 158 oceanic forcing for all GCMs considered here. A noteworthy aspect is that the cumulative SMB anomaly  
 159 can be both positive and negative. This is a consequence of the counteracting effects of increasing loss (pre-  
 160 cipitation, evaporation), but also increasing precipitation due to larger moisture transport by the warmer  
 161 air. The different GCMs predict a different net effect on the SMB, ranging from distinctly positive to  
 162 distinctly negative.

163 While the climate indices are based on results from a single GCM (MIROC4m), a strength of our  
 164 method is that it does not depend too much on the sensitivity of this particular model to changed external  
 165 forcing (“climate sensitivity”). This is so because of the normalization carried out by Eq. (1), which  
 166 eliminates at least the linear part of the climate sensitivity. The extrapolation of Eq. (2) makes sure  
 167 that the normalization also holds for RCP2.6, even though we do not have MIROC4m results for this  
 168 pathway. Therefore, the extrapolation, even though ad hoc, is not too critical. It mainly affects the long-  
 169 term behaviour, for which it produces the plausible result that, while for RCP8.5 climate change continues

170 beyond 2100, for RCP2.6 a partial recovery occurs.

For one of the ISMIP6 simulations (CCSM4/RCP8.5), an additional ice-shelf-collapse forcing is employed. It stipulates that ice-shelf collapse occurs when the mean surface melting over the past decade exceeds a threshold value of 725 mm water equiv.  $\text{a}^{-1}$  (Trusel and others, 2015; Seroussi and others, 2020). Hereby, the mean surface melting is parameterized by an exponential function of the DJF (austral summer) near-surface air temperature,  $ST\_DJF$ . For  $t \leq 2100$  CE,  $ST\_DJF$  is taken from bias-adjusted, GCM-forced simulations with the regional climate model RACMO2 (Trusel and others, 2015). For  $t > 2100$  CE, we construct  $ST\_DJF$  via its anomaly,  $\Delta ST\_DJF$ , as follows:

$$\begin{aligned} \Delta ST\_DJF(x, y, t) &= c_{ST\_DJF}(t) \times \Delta ST_{2091-2100}(x, y), \\ ST\_DJF(x, y, t) &= ST_{1995-2014}(x, y) \\ &\quad + [ST\_DJF_{\text{param}}(x, y) - ST_{\text{param}}(x, y)] \\ &\quad + \Delta ST\_DJF(x, y, t), \end{aligned} \quad t > 2100 \text{ CE.} \quad (7)$$

171 Note that  $\Delta ST_{2091-2100}$  and  $ST_{1995-2014}$  are mean-annual rather than DJF values because only these are  
172 available in the ISMIP6 forcing. To convert to DJF, we use the parameterized difference  $[ST\_DJF_{\text{param}} -$   
173  $ST_{\text{param}}]$  of present-day DJF and mean-annual temperatures, respectively, by Fortuin and Oerlemans (1990)  
174 (see also Greve and others, 2020a, their Eqs. (10) and (11)).

175 This method provides annual ice-shelf-collapse masks for the years 2101–2300. To guarantee a smooth  
176 transition to the pre-2100 masks provided by ISMIP6, we define a 10-year interval 2101–2110, during which  
177 the final masks are computed as weighted averages between the original ISMIP6 masks and our extended  
178 ones.

### 179 3 MODEL EXPERIMENTS

180 We apply the ice-sheet model SICOPOLIS (SICOPOLIS Authors, 2021) to the AIS with hybrid shallow-ice-  
181 shelfy-stream dynamics (Bernales and others, 2017) for grounded ice, shallow-shelf dynamics for floating  
182 ice, a Weertman-Budd-type sliding law tuned separately for 18 different regions (Greve and others, 2020a),  
183 and ice thermodynamics treated by the one-layer melting-CTS enthalpy scheme (CTS: cold-temperate  
184 transition surface; Blatter and Greve, 2015; Greve and Blatter, 2016). The horizontal resolution is 8 km,  
185 which, in combination with the sliding law that features a continuous basal drag across the grounding

line, is sufficient to produced good results for the grounding line migration in both advance and retreat scenarios (Gladstone and others, 2017; Chambers and others, 2022). In the vertical, we use terrain-following coordinates (sigma transformation) with 81 layers in the ice domain and 41 layers in the thermal lithosphere layer below. For details on the set-up, the initialization procedure by a paleoclimatic spin-up, comparisons between the simulated and observed ice thickness and surface velocity for our initialization year 1990, as well as the historical run (“hist”) that bridges the gap between 1990 and the start date of the projections in January 2015 by employing NorESM1-M/RCP8.5 surface mass balance (SMB), surface temperature (ST) and oceanic thermal forcing (TF), we refer to Greve and others (2020a). From the last 20 years of the historical run, we extract the 1995–2014 climatology (SMB, ST) required as a reference for the future climate experiments.

An overview of our extended ISMIP6 experiments is given in Table 2. The method of extending the ISMIP6 climate forcing until 2300 is described above (Sect. 2). 14 experiments are for the 21st-century unabated warming pathway RCP8.5 (CMIP5) / SSP5-8.5 (CMIP6), and three are for the reduced emissions pathway RCP2.6 (CMIP5) / SSP1-2.6 (CMIP6) that is largely in line with the commitments of the Paris Agreement (maintaining the global mean temperature well below a 2°C increase above pre-industrial levels). In two of the RCP8.5 experiments, the impact of different calibrations of the parameterization for sub-ice-shelf melting (“high” and “low” vs. the normal, “medium” calibration, thereby exploring the uncertainty of the parameterization) is tested, and one experiment employs a calibration in which only observed basal-melt values near the grounding line of the Pine Island ice shelf are used (“PIGL-medium”) (Jourdain and others, 2020). As already mentioned in Sect. 2.2, in one experiment, ice-shelf fracture triggered by surface melting is accounted for. In addition, a projection control simulation (“ctrl\_proj”) employs constant climate conditions based on the 1995–2014 reference climatology.

## 4 RESULTS

The simulated mass change of the AIS, expressed as a sea-level contribution, is shown in Figure 2. For the control run ctrl\_proj, the ice sheet remains stable, showing only a minimal mass loss of 3.49 mm SLE during the 286 years model time. This stability also holds for the longer control run over a 986-years period until the year 3000 reported by Chambers and others (2022).

Until 2100, the future projections are equivalent to the original ISMIP6-Antarctica simulations carried out with SICOPOLIS (Seroussi and others, 2020; Greve and others, 2020a; Payne and others, 2021),

215 characterized by a range of uncertainties from a notable mass loss to a slight mass gain and no clear  
216 separation between RCP8.5/SSP5-8.5 (mean  $\pm$  1-sigma range:  $32.6 \pm 67.2$  mm SLE) and RCP2.6/SSP1-2.6  
217 ( $8.4 \pm 15.9$  mm SLE). [Note: The values for RCP8.5/SSP5-8.5 differ from those given by Greve and others  
218 (2020a) because that study excluded Exp. 13 (NorESM1-M/RCP8.5 with “PIGL-medium” calibration) for  
219 the computation, which we have included here.] However, a different picture emerges in the longer term.  
220 By 2300, the ice sheet ends up losing mass for all cases, and it responds much more strongly to the ensemble  
221 of RCP8.5/SSP5-8.5 simulations than to the RCP2.6/SSP1-2.6 simulations. The final mass loss amounts  
222 to  $1.54 \pm 0.84$  m SLE for RCP8.5/SSP5-8.5, while it is limited to  $0.164 \pm 0.049$  m SLE for RCP2.6/SSP1-2.6.  
223 The mean values for both pathways are approximately twice as large as those found by Chambers and  
224 others (2022) for a sustained late-21st-century climate (no further warming trend) beyond 2100 (Fig. 2b).

225 The influence of the ice mass loss due to oceanic forcing is explored by Exps. 5, 9, 10 (NorESM1-  
226 M/RCP8.5 with “medium”, “high” and “low” calibration, respectively). The results are shown by the olive  
227 lines and olive-shaded regions in Figure 2. By 2300, the simulated mass loss is  $1.43^{+0.31}_{-0.20}$  m SLE. Thus,  
228 the uncertainty due to these three calibrations is significant, but smaller than the uncertainty due to the  
229 GCM forcings. A more extreme test is Exp. 13, which is NorESM1-M/RCP8.5 with the “PIGL-medium”  
230 calibration. Until the mid-22nd century, this leads to an, on average,  $\sim 2$  times larger total ice-shelf  
231 basal melting than for Exp. 5 (later on, the difference becomes smaller due to ice-shelf decay). It has a  
232 pronounced effect on the mass loss of the ice sheet: By 2300, it is 2.97 m SLE compared to the initial 1990  
233 state, more than doubling that of Exp.5. This highlights the great sensitivity of the AIS to oceanic forcing.

234 Exps. 8 and 12 (CCSM4/RCP8.5) investigate the influence of ice-shelf hydrofracture as described above  
235 (included in Exp. 12). Exp. 8 is actually one of the cases that produce a mass gain of the ice sheet during  
236 the 21st century. Adding ice-shelf hydrofracture via the time-dependent collapse mask in Exp. 12 reverts  
237 this behaviour to a mass loss. By 2300, both experiments produce a loss, which is 1.27 m SLE for Exp. 8,  
238 but 2.00 m SLE for Exp. 12. Thus, the process can act as a significant amplifier of the mass loss of the AIS.

239 In Figure 3, the sea-level contributions by 2300 are shown separately for the regions of the EAIS, the  
240 WAIS and the Antarctic Peninsula (AP). Averaged across all the high-emission cases (panel a), the WAIS  
241 contributes 1.28 m SLE, compared with just 0.24 m SLE from the EAIS and 0.019 m SLE from the AP. This  
242 contrasts with the low-emission cases (panel b) which have average SLE contributions from the WAIS  
243 and EAIS of 0.064 and 0.097 m, respectively, with the AP contribution being very slightly negative at  
244  $-0.00078$  m. These findings agree with those by Chambers and others (2022) (simulations until 3000, no

245 further warming or cooling trend beyond 2100), and the reason for the predominant contribution from the  
246 WAIS for RCP8.5/SSP5-8.5 is that it undergoes a MISI in the areas of the Amundsen Sea Embayment and  
247 the Siple Coast where the bedrock bathymetry deepens inward. By contrast, the weaker climatic forcings  
248 of RCP2.6/SSP1-2.6 do not trigger the WAIS instability in our simulations.

249 We now discuss in more detail the results of Exp. 6 (MIROC-ESM-CHEM/RCP8.5), which was already  
250 focused on in the previous study by Chambers and others (2022). It features high atmospheric changes and  
251 median ocean warming compared to the other CMIP5 GCMs (Barthel and others, 2020), and it produces  
252 a  $\sim 29\%$  above average mass loss of 1.99 m SLE (WAIS 1.69 m, EAIS 0.16 m, AP 0.13 m) for our combined  
253 CMIP5/CMIP6 ensemble. Figure 4 shows the components of the global mass balance (integrated over the  
254 ice sheet, all counted as positive for mass gain): surface mass balance (SMB), basal mass balance (BMB),  
255 calving and ice volume change ( $dV/dt$ ). The residual,  $\text{Res} = |\text{SMB} + \text{BMB} + \text{Calving} - dV/dt|$ , has a mean  
256 value of  $2.14 \times 10^4 \text{ m}^3 \text{ a}^{-1}$  over the 286 years simulation time. This is eight orders of magnitude smaller  
257 than the typical range of values in the figure [ $\mathcal{O}(10^{12} \text{ m}^3 \text{ a}^{-1})$ ], so that the model conserves mass very well  
258 (see also Calov and others, 2018).

259 The ice sheet keeps losing volume ( $\propto$  mass) over the entire period and at an accelerating rate of change.  
260 The SMB, driven by the counteracting effects of increasing precipitation and increasing runoff, remains  
261 positive throughout the model time. The BMB, predominantly produced by sub-ice-shelf melting, strongly  
262 increases in magnitude over time, which is the main reason for the accelerated volume loss of the ice sheet.  
263 The essentially monotonic increase (except for short-term fluctuations) of the BMB contrasts with the  
264 study by Chambers and others (2022) where it peaks around 2100, but then falls back to values around  
265  $-4 \times 10^{12} \text{ m}^3 \text{ a}^{-1}$  between 2150 and 2300. Calving into the surrounding ocean (that results from a 50-  
266 m ice-thickness threshold; Greve and others, 2020a) is also a significant component of the mass balance.  
267 However, it changes only moderately over time, except for a period of increased calving with a peak around  
268 2170 due to a major retreat event of the Ross Ice Shelf. The inter-annual variability of the volume change is  
269 mainly due to that of the SMB and the BMB, which reflects the variability of the atmospheric and oceanic  
270 forcings.

271 In Appendix A, we present a similar analysis of the global mass balance for the pair of Exps. 5 and 7  
272 (NorESM1-M/RCP8.5, NorESM1-M/RCP2.6).

273 Snapshots of the simulated ice thickness and surface velocity for Exp. 6 are shown in Figure 5. By 2095,  
274 the ice sheet has overall undergone only minor changes compared to the initial year 2015, corresponding to a

275 mass loss of 0.0070 m SLE. By 2195, which is just after the calving event mentioned above, the changes are  
276 more notable (mass loss 0.40 m SLE). A large part of the present-day Ross Ice Shelf has disappeared, and  
277 the grounding lines in the areas of the Pine Island and Thwaites glaciers and the Siple Coast have migrated  
278 inland, along with a speed-up of the ice streams. A similar, yet less pronounced grounding line retreat  
279 and speed-up has occurred in the area of Totten Glacier, and the northern part of the Amery Ice Shelf has  
280 disintegrated. By the end of 2300 (mass loss 1.99 m SLE), the instability of the WAIS is progressing in full  
281 force, with dramatic retreats of the Pine Island/Thwaites and Siple Coast grounding lines, accompanied by  
282 additional retreats of the grounding line of the Filchner–Ronne Ice Shelf. In the EAIS, the Amery Ice Shelf  
283 has disappeared almost entirely, and the area of Totten Glacier shows some more grounding line retreat;  
284 however, with limited impact on the ice sheet further inland.

## 285 5 DISCUSSION AND CONCLUSION

286 The future climate simulations for the AIS until the year 2300 carried out in the present study reveal a  
287 different picture compared to the original ISMIP6-Antarctica simulations for the 21st century (Seroussi  
288 and others, 2020; Greve and others, 2020a; Payne and others, 2021). The latter produced a range of mass  
289 changes from a small gain (due to precipitation increases) to a moderate loss, and no clear distinction  
290 between the unabated warming (RCP8.5/SSP5-8.5) and reduced emissions pathways (RCP2.6/SSP1-2.6).  
291 By contrast, in our extended simulations, by 2300 mass gains of the AIS do not occur any more, and the  
292 mass loss under RCP8.5/SSP5-8.5 is substantially larger than that under RCP2.6/SSP1-2.6 (mean values  
293 of  $\sim 1.5$  m SLE vs. only  $\sim 0.16$  m SLE). In terms of the mean  $\pm 1$ -sigma mass loss range, RCP8.5/SSP5-8.5  
294 becomes disjoint from RCP2.6/SSP1-2.6 around the year 2208. For comparison, Lowry and others (2021)  
295 report for their projections, based on a statistical emulator, “likely” and “very likely” times of emergence  
296 (significant separation between the RCP8.5 and RCP2.6 ensembles) of 2116 and 2189, respectively. Most  
297 of the mass loss under RCP8.5/SSP5-8.5 originates from the WAIS, which suffers a MISI in almost all  
298 simulations.

299 Compared to the previous study by Chambers and others (2022) in which a sustained late-21st-century  
300 climate beyond 2100 was assumed, the response of the AIS to our extrapolated climate-change scenarios  
301 is about two times larger by 2300 for both pathways. For RCP8.5/SSP5-8.5, this stronger response is  
302 immediately to be expected because, as detailed in Sect. 2.1, all climate indices are well above unity during  
303 the 22nd and 23rd century, which means that climate change becomes ever more serious. For RCP2.6/SSP1-

304 2.6, the situation is different because the atmospheric climate recovers to below late-21st-century levels (all  
305 five indices), while only the the oceanic climate index stays above unity after 2100. Evidently, the impact  
306 of the increasing oceanic forcing outweighs that of the recovering atmospheric forcing, so that mass loss  
307 due to sub-ice-shelf melt and subsequently enhanced drainage of grounded ice is the dominant process.

308 The threat of a WAIS instability under future climate change has already been expressed by a number  
309 of previous studies (see Sect. 1 for more details). A particular feature of the ISMIP6-Antarctica set-up for  
310 SICOPOLIS is that it applies an SMB correction to keep the ice sheet stable and close to observed conditions  
311 in the recent past (Greve and others, 2020a). This SMB correction has significant additional accumulation  
312 in the area of the Pine Island and Thwaites glaciers to prevent them from becoming unstable even before  
313 the end of the spin-up simulations. It is possible that this procedure over-stabilizes the area, so that the  
314 onset of the instability originating from there could be delayed. On the other hand, SICOPOLIS is quite  
315 sensitive to sub-ice-shelf melting compared to other ice-sheet models (Edwards and others, 2021). This  
316 factor facilitates the development of a MISI because it makes the ice sheet more sensitive to grounding-line  
317 migration.

318 As already discussed by Chambers and others (2022), a weakness of the ISMIP6-type simulations is  
319 that the atmospheric forcing is not affected by the changing geometry of the ice sheet. While the ocean  
320 thermal forcing, TF, is three-dimensional and thus changes as the ice shelves become thicker or thinner,  
321 the atmospheric forcing fields,  $\Delta ST$  and  $\Delta SMB$ , are 2D fields that were derived by GCMs under the  
322 assumption of a static, present-day ice sheet. Therefore, they do not change as the ice-surface elevation  
323 rises or falls. A possible improvement, also beneficial for the resolution of the forcing fields, is to reprocess  
324 the GCM output by a regional climate model and compute vertical gradients of ST and SMB, so that at  
325 least a linearized feedback can be implemented (Franco and others, 2012). Such a method was employed  
326 for the ISMIP6-Greenland simulations and derived work (Goelzer and others, 2020; Nowicki and others,  
327 2020; Greve and Chambers, 2022). Short of very demanding and computationally expensive fully coupled  
328 climate–ice-sheet simulations, a further possibility is to involve snapshots of climate-model results combined  
329 with more refined parameterizations for the climatic forcing, similar to the approach by Abe-Ouchi and  
330 others (2013) for the paleoglaciation of the Northern Hemisphere.

331 Furthermore, future work in the direction of long-term simulations of ice-sheet response to climate  
332 change should aim at employing more direct, rather than extrapolated, GCM projections beyond 2100  
333 and involving an ensemble of ice-sheet models to allow an improved assessment of uncertainties. Within

334 ISMIP6, this is currently planned within a new initiative “ISMIP6-Projections2300-Antarctica” for the AIS  
335 ([tinyurl.com/ismip6-ais-2300](https://tinyurl.com/ismip6-ais-2300), last access: 2022-05-11). In detail, this initiative focuses on projections ex-  
336 tended until 2300 (as in the present study) based on CMIP5 and CMIP6 GCM outputs. Some experiments  
337 will use repeated climate forcing from the late 21st century, sampled randomly between 2100 and 2300  
338 (similar to the approach by Chambers and others, 2022), while others will be based on output from GCMs  
339 directly run until 2300 under CMIP forcing pathways. We will contribute to these projections with the  
340 SICOPOLIS model.

#### 341 **CODE AND DATA AVAILABILITY**

342 SICOPOLIS (SICOPOLIS Authors, 2021) is free and open-source software, published on a persistent Git  
343 repository hosted by the Alfred Wegener Institute for Polar and Marine Research (AWI) in Bremerhaven,  
344 Germany (<https://gitlab.awi.de/sicopolis/sicopolis/>). The output data produced for this study are avail-  
345 able at Zenodo, <https://doi.org/10.5281/zenodo.xxxxxxx> [NOT YET AVAILABLE].

#### 346 **AUTHOR CONTRIBUTIONS**

347 Ralf Greve, Christopher Chambers and Ayako Abe-Ouchi designed the study. Takashi Obase, Fuyuki Saito,  
348 Wing-Le Chan and Ayako Abe-Ouchi ran the MIROC simulations. Ralf Greve, Christopher Chambers and  
349 Takashi Obase computed the climate indices and the extrapolated ISMIP6 climate forcing. Ralf Greve  
350 ran the SICOPOLIS simulations with support from Christopher Chambers. All authors discussed and  
351 interpreted the results. Ralf Greve wrote the manuscript with contributions from all authors.

#### 352 **ACKNOWLEDGEMENTS**

353 We thank the Scientific Editor Frank Pattyn and two reviewers for constructive remarks and suggestions  
354 that helped to improve the manuscript. We thank Jorge Bernales (Utrecht University) and Reinhard  
355 Calov (PIK Potsdam) for their recent contributions to the development of the SICOPOLIS model. Some  
356 colour schemes of our figures were taken from Paul Tol’s (SRON Netherlands Institute for Space Research)  
357 online resource at <https://personal.sron.nl/~pault> (last access: 2022-05-11). We thank the Climate and  
358 Cryosphere (CliC) effort, which provided support for ISMIP6 through sponsoring of workshops, hosting  
359 the ISMIP6 website and wiki, and promoting ISMIP6. We acknowledge the World Climate Research



360 Programme, which, through its Working Group on Coupled Modelling, coordinated and promoted CMIP5  
361 and CMIP6. We thank the climate modelling groups for producing their model output and making it  
362 available; the Earth System Grid Federation (ESGF) for archiving the CMIP data and providing access to  
363 it; the University at Buffalo for ISMIP6 data distribution and upload; and the multiple funding agencies  
364 who support CMIP5, CMIP6, and ESGF. We thank the ISMIP6 steering committee, the ISMIP6 model  
365 selection group and ISMIP6 dataset preparation group for their continuous engagement in defining ISMIP6.  
366 This is ISMIP6 contribution No. 28.

367 *Financial support.* Ralf Greve, Christopher Chambers, Wing-Le Chan and Ayako Abe-Ouchi were  
368 supported by Japan Society for the Promotion of Science (JSPS) KAKENHI Grant No. JP17H06323. Ralf  
369 Greve, Wing-Le Chan and Ayako Abe-Ouchi were supported by JSPS KAKENHI Grant No. JP17H06104.  
370 Takashi Obase, Fuyuki Saito and Ayako Abe-Ouchi were supported by JSPS Grant-in-Aid for Japan–France  
371 Integrated Action Program (SAKURA Program) No. JPJSBP120213203.

## 372 REFERENCES

- 373 Abe-Ouchi A, Saito F, Kawamura K, Raymo ME, Okuno J, Takahashi K and Blatter H (2013) Insolation-driven  
374 100,000-year glacial cycles and hysteresis of ice-sheet volume. *Nature*, **500**(7461), 190–193 (doi: 10.1038/nature12374)  
375
- 376 Alley RB, Anandakrishnan S, Christianson K, Horgan HJ, Muto A, Parizek BR, Pollard D and Walker RT (2015)  
377 Oceanic forcing of ice-sheet retreat: West Antarctica and more. *Annual Review of Earth and Planetary Sciences*,  
378 **43**(1), 207–231 (doi: 10.1146/annurev-earth-060614-105344)
- 379 Bakker P, Schmittner A, Lenaerts JTM, Abe-Ouchi A, Bi D, van den Broeke MR, Chan WL, Hu A, Beadling RL,  
380 Marsland SJ, Mernild SH, Saenko OA, Swingedouw D, Sullivan A and Yin J (2016) Fate of the Atlantic Meridional  
381 Overturning Circulation: Strong decline under continued warming and Greenland melting. *Geophysical Research*  
382 *Letters*, **43**, 12252–12260 (doi: 10.1002/2016GL070457)
- 383 Barthel A, Agosta C, Little CM, Hattermann T, Jourdain NC, Goelzer H, Nowicki S, Seroussi H, Straneo F and  
384 Bracegirdle TJ (2020) CMIP5 model selection for ISMIP6 ice sheet model forcing: Greenland and Antarctica. *The*  
385 *Cryosphere*, **14**(3), 855–879 (doi: 10.5194/tc-14-855-2020)
- 386 Bernales J, Rogozhina I, Greve R and Thomas M (2017) Comparison of hybrid schemes for the combination of  
387 shallow approximations in numerical simulations of the Antarctic Ice Sheet. *The Cryosphere*, **11**(1), 247–265 (doi:  
388 10.5194/tc-11-247-2017)

- 389 Blatter H and Greve R (2015) Comparison and verification of enthalpy schemes for polythermal glaciers and ice  
390 sheets with a one-dimensional model. *Polar Science*, **9**(2), 196–207 (doi: 10.1016/j.polar.2015.04.001)
- 391 Bulthuis K, Arnst M, Sun S and Pattyn F (2019) Uncertainty quantification of the multi-centennial response of the  
392 Antarctic ice sheet to climate change. *The Cryosphere*, **13**(4), 1349–1380 (doi: 10.5194/tc-13-1349-2019)
- 393 Calov R, Beyer S, Greve R, Beckmann J, Willeit M, Kleiner T, Rückamp M, Humbert A and Ganopolski A (2018)  
394 Simulation of the future sea level contribution of Greenland with a new glacial system model. *The Cryosphere*,  
395 **12**(10), 3097–3121 (doi: 10.5194/tc-12-3097-2018)
- 396 Chambers C, Greve R, Obase T, Saito F and Abe-Ouchi A (2022) Mass loss of the Antarctic ice sheet un-  
397 til the year 3000 under a sustained late-21st-century climate. *Journal of Glaciology*, **68**(269), 605–617 (doi:  
398 10.1017/jog.2021.124)
- 399 DeConto RM, Pollard D, Alley RB, Velicogna I, Gasson E, Gomez N, Sadai S, Condron A, Gilford DM, Ashe EL,  
400 Kopp RE, Li D and Dutton A (2021) The Paris Climate Agreement and future sea-level rise from Antarctica.  
401 *Nature*, **593**(7857), 83–89 (doi: 10.1038/s41586-021-03427-0)
- 402 Dutton A, Carlson AE, Long AJ, Milne GA, Clark PU, DeConto R, Horton BP, Rahmstorf S and Raymo ME  
403 (2015) Sea-level rise due to polar ice-sheet mass loss during past warm periods. *Science*, **349**(6244), aaa4019 (doi:  
404 10.1126/science.aaa4019)
- 405 Edwards TL, Nowicki S, Marzeion B, Hock R, Goelzer H, Seroussi H, Jourdain NC, Slater DA, Turner FE, Smith CJ,  
406 McKenna CM, Simon E, Abe-Ouchi A, Gregory JM, Larour E, Lipscomb WH, Payne AJ, Shepherd A, Agosta C,  
407 Alexander P, Albrecht T, Anderson B, Asay-Davis X, Aschwanden A, Barthel A, Bliss A, Calov R, Chambers C,  
408 Champollion N, Choi Y, Cullather R, Cuzzzone J, Dumas C, Felikson D, Fettweis X, Fujita K, Galton-Fenzi BK,  
409 Gladstone R, Golledge NR, Greve R, Hattermann T, Hoffman MJ, Humbert A, Huss M, Huybrechts P, Immerzeel  
410 W, Kleiner T, Kraaijenbrink P, Le clec'h S, Lee V, Leguy GR, Little CM, Lowry DP, Malles JH, Martin DF,  
411 Maussion F, Morlighem M, O'Neill JF, Nias I, Pattyn F, Pelle T, Price SF, Quiquet A, Radić V, Reese R, Rounce  
412 DR, Rückamp M, Sakai A, Shafer C, Schlegel NJ, Shannon S, Smith RS, Straneo F, Sun S, Tarasov L, Trusel LD,  
413 Van Breedam J, van de Wal R, van den Broeke M, Winkelmann R, Zekollari H, Zhao C, Zhang T and Zwinger  
414 T (2021) Projected land ice contributions to twenty-first-century sea level rise. *Nature*, **593**(7857), 74–82 (doi:  
415 10.1038/s41586-021-03302-y)
- 416 Eyring V, Bony S, Meehl GA, Senior CA, Stevens B, Stouffer RJ and Taylor KE (2016) Overview of the Coupled Model  
417 Intercomparison Project Phase 6 (CMIP6) experimental design and organization. *Geoscientific Model Development*,  
418 **9**(5), 1937–1958 (doi: 10.5194/gmd-9-1937-2016)

- 419 Fortuin JPF and Oerlemans J (1990) Parameterization of the annual surface temperature and mass balance of  
420 Antarctica. *Annals of Glaciology*, **14**, 78–84 (doi: 10.3189/S0260305500008302)
- 421 Franco B, Fettweis X, Lang C and Erpicum M (2012) Impact of spatial resolution on the modelling of the Greenland  
422 ice sheet surface mass balance between 1990–2010, using the regional climate model MAR. *The Cryosphere*, **6**(3),  
423 695–711 (doi: 10.5194/tc-6-695-2012)
- 424 Garbe J, Albrecht T, Levermann A, Donges JF and Winkelmann R (2020) The hysteresis of the Antarctic Ice Sheet.  
425 *Nature*, **585**(7826), 538–544 (doi: 10.1038/s41586-020-2727-5)
- 426 Gasson E, DeConto RM, Pollard D and Levy RH (2016) Dynamic Antarctic ice sheet during the early to mid-  
427 Miocene. *Proceedings of the National Academy of Sciences of the United States of America*, **113**(13), 3459–3464  
428 (doi: 10.1073/pnas.1516130113)
- 429 Gladstone RM, Warner RC, Galton-Fenzi BK, Gagliardini O, Zwinger T and Greve R (2017) Marine ice sheet  
430 model performance depends on basal sliding physics and sub-shelf melting. *The Cryosphere*, **11**(1), 319–329 (doi:  
431 10.5194/tc-11-319-2017)
- 432 Goelzer H, Nowicki S, Payne A, Larour E, Seroussi H, Lipscomb WH, Gregory J, Abe-Ouchi A, Shepherd A, Simon E,  
433 Agosta C, Alexander P, Aschwanden A, Barthel A, Calov R, Chambers C, Choi Y, Cuzzzone J, Dumas C, Edwards  
434 T, Felikson D, Fettweis X, Golledge NR, Greve R, Humbert A, Huybrechts P, Le clec'h S, Lee V, Leguy G, Little  
435 C, Lowry DP, Morlighem M, Nias I, Quiquet A, Rückamp M, Schlegel NJ, Slater D, Smith R, Straneo F, Tarasov  
436 L, van de Wal R and van den Broeke M (2020) The future sea-level contribution of the Greenland ice sheet: a  
437 multi-model ensemble study of ISMIP6. *The Cryosphere*, **14**(9), 3071–3096 (doi: 10.5194/tc-14-3071-2020)
- 438 Golledge NR, Kowalewski DE, Naish TR, Levy RH, Fogwill CJ and Gasson EGW (2015) The multi-millennial  
439 Antarctic commitment to future sea-level rise. *Nature*, **526**(7573), 421–425 (doi: 10.1038/nature15706)
- 440 Greve R and Blatter H (2016) Comparison of thermodynamics solvers in the polythermal ice sheet model SICOPOLIS.  
441 *Polar Science*, **10**(1), 11–23 (doi: 10.1016/j.polar.2015.12.004)
- 442 Greve R and Chambers C (2022) Mass loss of the Greenland ice sheet until the year 3000 under a sustained late-  
443 21st-century climate. *Journal of Glaciology*, **68**(269), 618–624 (doi: 10.1017/jog.2022.9)
- 444 Greve R, Calov R, Obase T, Saito F, Tsutaki S and Abe-Ouchi A (2020a) ISMIP6 future projections for the Antarctic  
445 ice sheet with the model SICOPOLIS. Technical report, Zenodo (doi: 10.5281/zenodo.3971232)
- 446 Greve R, Chambers C and Calov R (2020b) ISMIP6 future projections for the Greenland ice sheet with the model  
447 SICOPOLIS. Technical report, Zenodo (doi: 10.5281/zenodo.3971251)

- 448 IPCC (2021) *Climate Change 2021: The Physical Science Basis. Contribution of Working Group I to the Sixth*  
449 *Assessment Report of the Intergovernmental Panel on Climate Change*. Cambridge University Press, Cambridge,  
450 UK and New York, NY, USA, URL: <https://www.ipcc.ch/report/ar6/wg1/>
- 451 Joughin I, Smith BE and Medley B (2014) Marine ice sheet collapse potentially under way for the Thwaites Glacier  
452 Basin, West Antarctica. *Science*, **344**(6185), 735–738 (doi: 10.1126/science.1249055)
- 453 Jourdain NC, Asay-Davis X, Hattermann T, Straneo F, Seroussi H, Little CM and Nowicki S (2020) A protocol for  
454 calculating basal melt rates in the ISMIP6 Antarctic ice sheet projections. *The Cryosphere*, **14**(9), 3111–3134 (doi:  
455 10.5194/tc-14-3111-2020)
- 456 Levermann A, Clark PU, Marzeion B, Milne GA, Pollard D, Radic V and Robinson A (2013) The multimillennial  
457 sea-level commitment of global warming. *Proceedings of the National Academy of Sciences of the United States of*  
458 *America*, **110**(34), 13745–13750 (doi: 10.1073/pnas.1219414110)
- 459 Lipscomb WH, Leguy GR, Jourdain NC, Asay-Davis X, Seroussi H and Nowicki S (2021) ISMIP6-based projections of  
460 ocean-forced Antarctic Ice Sheet evolution using the Community Ice Sheet Model. *The Cryosphere*, **15**(2), 633–661  
461 (doi: 10.5194/tc-15-633-2021)
- 462 Lowry DP, Krapp M, Golledge NR and Alevropoulos-Borrill A (2021) The influence of emissions scenarios on fu-  
463 ture Antarctic ice loss is unlikely to emerge this century. *Communications Earth & Environment*, **2**, 221 (doi:  
464 10.1038/s43247-021-00289-2)
- 465 Mercer JH (1978) West Antarctic ice sheet and CO<sub>2</sub> greenhouse effect: a threat of disaster. *Nature*, **271**(5643),  
466 321–325 (doi: 10.1038/271321a0)
- 467 Morlighem M, Williams CN, Rignot E, An L, Arndt JE, Bamber JL, Catania G, Chauché N, Dowdeswell JA, Dorschel  
468 B, Fenty I, Hogan K, Howat I, Hubbard A, Jakobsson M, Jordan TM, Kjeldsen KK, Millan R, Mayer L, Mouginot  
469 J, Noël BPY, O’Cofaigh C, Palmer S, Rysgaard S, Seroussi H, Siegert MJ, Slabon P, Straneo F, van den Broeke  
470 MR, Weinrebe W, Wood M and Zinglensen KB (2017) BedMachine v3: Complete bed topography and ocean  
471 bathymetry mapping of Greenland from multibeam echo sounding combined with mass conservation. *Geophysical*  
472 *Research Letters*, **44**(21), 11051–11061 (doi: 10.1002/2017GL074954)
- 473 Morlighem M, Rignot E, Binder T, Blankenship D, Drews G, Rand Eagles, Eisen O, Ferraccioli F, Forsberg R, Fretwell  
474 P, Goel V, Greenbaum JS, Gudmundsson H, Guo J, Helm V, Hofstede C, Howat I, Humbert A, Jokat W, Karlsson  
475 NB, Lee WS, Matsuoka K, Millan R, Mouginot J, Paden J, Pattyn F, Roberts J, Rosier S, Ruppel A, Seroussi H,  
476 Smith EC, Steinhage D, Sun B, van den Broeke MR, van Ommen TD, van Wessem M and Young DA (2020) Deep  
477 glacial troughs and stabilizing ridges unveiled beneath the margins of the Antarctic ice sheet. *Nature Geoscience*,  
478 **13**(2), 132–137 (doi: 10.1038/s41561-019-0510-8)

- 479 Nowicki S, Goelzer H, Seroussi H, Payne AJ, Lipscomb WH, Abe-Ouchi A, Agosta C, Alexander P, Asay-Davis  
480 XS, Barthel A, Bracegirdle TJ, Cullather R, Felikson D, Fettweis X, Gregory JM, Hattermann T, Jourdain NC,  
481 Kuipers Munneke P, Larour E, Little CM, Morlighem M, Nias I, Shepherd A, Simon E, Slater D, Smith RS, Straneo  
482 F, Trusel LD, van den Broeke MR and van de Wal R (2020) Experimental protocol for sea level projections from  
483 ISMIP6 stand-alone ice sheet models. *The Cryosphere*, **14**(7), 2331–2368 (doi: 10.5194/tc-14-2331-2020)
- 484 Nowicki SMJ, Payne A, Larour E, Seroussi H, Goelzer H, Lipscomb W, Gregory J, Abe-Ouchi A and Shepherd A  
485 (2016) Ice Sheet Model Intercomparison Project (ISMIP6) contribution to CMIP6. *Geoscientific Model Develop-*  
486 *ment*, **9**(12), 4521–4545 (doi: 10.5194/gmd-9-4521-2016)
- 487 Payne AJ, Nowicki S, Abe-Ouchi A, Agosta C, Alexander P, Albrecht T, Asay-Davis X, Aschwanden A, Barthel  
488 A, Bracegirdle TJ, Calov R, Chambers C, Choi Y, Cullather R, Cuzzone J, Dumas C, Edwards TL, Felikson  
489 D, Fettweis X, Galton-Fenzi BK, Goelzer H, Gladstone R, Golledge NR, Gregory JM, Greve R, Hattermann T,  
490 Hoffman MJ, Humbert A, Huybrechts P, Jourdain NC, Kleiner T, Kuipers Munneke P, Larour E, Le clec'h S, Lee  
491 V, Leguy G, Lipscomb WH, Little CM, Lowry DP, Morlighem M, Nias I, Pattyn F, Pelle T, Price SF, Quiquet  
492 A, Reese R, Rückamp M, Schlegel NJ, Seroussi H, Shepherd A, Simon E, Slater D, Smith RS, Straneo F, Sun  
493 S, Tarasov L, Trusel LD, Van Breedam J, van de Wal R, van den Broeke M, Winkelmann R, Zhao C, Zhang T  
494 and Zwinger T (2021) Future sea level change under Coupled Model Intercomparison Project Phase 5 and Phase  
495 6 scenarios from the Greenland and Antarctic ice sheets. *Geophysical Research Letters*, **48**(16), e2020GL091741  
496 (doi: 10.1029/2020GL091741)
- 497 Pollard D and DeConto RM (2009) Modelling West Antarctic ice sheet growth and collapse through the past five  
498 million years. *Nature*, **458**(7236), 329–332 (doi: 10.1038/nature07809)
- 499 Rignot E, Mouginot J, Morlighem M, Seroussi H and Scheuchl B (2014) Widespread, rapid grounding line retreat  
500 of Pine Island, Thwaites, Smith, and Kohler glaciers, West Antarctica, from 1992 to 2011. *Geophysical Research*  
501 *Letters*, **41**(10), 3502–3509 (doi: 10.1002/2014GL060140)
- 502 Schaeffer M, Hare W, Rahmstorf S and Vermeer M (2012) Long-term sea-level rise implied by 1.5°C and 2°C warming  
503 levels. *Nature Climate Change*, **2**(12), 867–870 (doi: 10.1038/nclimate1584)
- 504 Schoof C (2007) Ice sheet grounding line dynamics: Steady states, stability, and hysteresis. *Journal of Geophysical*  
505 *Research: Earth Surface*, **112**(F3), F03S28 (doi: 10.1029/2006JF000664)
- 506 Seroussi H, Nowicki S, Payne AJ, Goelzer H, Lipscomb WH, Abe-Ouchi A, Agosta C, Albrecht T, Asay-Davis X,  
507 Barthel A, Calov R, Cullather R, Dumas C, Galton-Fenzi BK, Gladstone R, Golledge N, Gregory JM, Greve R,  
508 Hatterman T, Hoffman MJ, Humbert A, Huybrechts P, Jourdain NC, Kleiner T, Larour E, Leguy GR, Lowry DP,  
509 Little CM, Morlighem M, Pattyn F, Pelle T, Price SF, Quiquet A, Reese R, Schlegel NJ, Shepherd A, Simon E,

- 510 Smith RS, Straneo F, Sun S, Trusel LD, Van Breedam J, van de Wal RSW, Winkelmann R, Zhao C, Zhang T and  
511 Zwinger T (2020) ISMIP6 Antarctica: a multi-model ensemble of the Antarctic ice sheet evolution over the 21st  
512 century. *The Cryosphere*, **14**(9), 3033–3070 (doi: 10.5194/tc-14-3033-2020)
- 513 SICOPOLIS Authors (2021) SICOPOLIS (version 5-dev, branch develop, commit hash cb5a75b9).  
514 GitLab, Alfred Wegener Institute for Polar and Marine Research, Bremerhaven, Germany, URL  
515 <https://gitlab.awi.de/sicopolis/sicopolis>
- 516 Sun S, Pattyn F, Simon EG, Albrecht T, Cornford S, Calov R, Dumas C, Gillet-Chaulet F, Goelzer H, Golledge NR,  
517 Greve R, Hoffman MJ, Humbert A, Kazmierczak E, Kleiner T, Leguy GR, Lipscomb WH, Martin D, Morlighem  
518 M, Nowicki S, Pollard D, Price S, Quiquet A, Seroussi H, Schlemm T, Sutter J, van de Wal RSW, Winkelmann R  
519 and Zhang T (2020) Antarctic ice sheet response to sudden and sustained ice-shelf collapse (ABUMIP). *Journal*  
520 *of Glaciology*, **66**(260), 891–904 (doi: 10.1017/jog.2020.67)
- 521 The IMBIE Team (2018) Mass balance of the Antarctic Ice Sheet from 1992 to 2017. *Nature*, **558**(7709), 219–222  
522 (doi: 10.1038/s41586-018-0179-y)
- 523 The IMBIE Team (2020) Mass balance of the Greenland Ice Sheet from 1992 to 2018. *Nature*, **579**(7798), 233–239  
524 (doi: 10.1038/s41586-019-1855-2)
- 525 Thomas RH and Bentley CR (1978) A model for Holocene retreat of the West Antarctic ice sheet. *Quaternary*  
526 *Research*, **10**(2), 150–170 (doi: 10.1016/0033-5894(78)90098-4)
- 527 Trusel LD, Frey KE, Das SB, Karnauskas KB, Kuipers Munneke P, van Meijgaard E and van den Broeke MR  
528 (2015) Divergent trajectories of Antarctic surface melt under two twenty-first-century climate scenarios. *Nature*  
529 *Geoscience*, **8**(12), 927–932 (doi: 10.1038/ngeo2563)
- 530 Turney CSM, Fogwill CJ, Golledge NR, McKay NP, van Sebille E, Jones RT, Etheridge D, Rubino M, Thornton DP,  
531 Davies SM, Ramsey CB, Thomas ZA, Bird MI, Munksgaard NC, Kohno M, Woodward J, Winter K, Weyrich LS,  
532 Rootes CM, Millman H, Albert PG, Rivera A, van Ommen T, Curran M, Moy A, Rahmstorf S, Kawamura K,  
533 Hillenbrand CD, Weber ME, Manning CJ, Young J and Cooper A (2020) Early Last Interglacial ocean warming  
534 drove substantial ice mass loss from Antarctica. *Proceedings of the National Academy of Sciences of the United*  
535 *States of America*, **117**(8), 3996–4006 (doi: 10.1073/pnas.1902469117)
- 536 Van Breedam J, Goelzer H and Huybrechts P (2020) Semi-equilibrated global sea-level change projections for the  
537 next 10 000 years. *Earth System Dynamics*, **11**(4), 953–976 (doi: 10.5194/esd-11-953-2020)
- 538 Weertman J (1974) Stability of the junction of an ice sheet and an ice shelf. *Journal of Glaciology*, **13**(67), 3–11 (doi:  
539 10.3189/S0022143000023327)

GCM	Scenario	$\overline{\Delta ST}$ (°C)	$c\Delta SMB$ (m ice equiv.)	$\overline{TF}$ (°C)
NorESM1-M	RCP8.5	5.667	15.510	2.209
MIROC-ESM-CHEM	RCP8.5	10.157	−6.325	1.442
NorESM1-M	RCP2.6	0.194	0.286	0.539
CCSM4	RCP8.5	9.511	19.375	1.652
HadGEM2-ES	RCP8.5	9.141	−62.238	2.391
CSIRO-Mk3.6.0	RCP8.5	9.654	33.240	1.381
IPSL-CM5A-MR	RCP8.5	6.351	23.166	1.247
IPSL-CM5A-MR	RCP2.6	0.515	0.612	0.709
CNRM-CM6-1	SSP5-8.5	12.435	44.911	1.927
CNRM-CM6-1	SSP1-2.6	1.245	2.587	0.827
UKESM1-0-LL	SSP5-8.5	11.102	−20.363	2.196
CESM2	SSP5-8.5	12.849	−22.145	1.613
CNRM-ESM2-1	SSP5-8.5	10.162	35.427	2.091

**Table 1.** Mean surface temperature anomaly ( $\overline{\Delta ST}$ ), cumulative SMB anomaly ( $c\Delta SMB$ ) and mean oceanic thermal forcing ( $\overline{TF}$ ) for the period 2015–2300 and all climate forcings of this study.  $\overline{\Delta ST}$  and  $c\Delta SMB$  spatially averaged over the present-day AIS (including ice shelves),  $\overline{TF}$  spatially averaged over the ice-shelf areas and the depth interval 200–800 m. Anomalies relative to 1995–2014 means of the reference climatology.

#	GCM	Scenario	Ocean forcing	Ice-shelf fracture		
0	—	ctrl_proj	—	—	Control experiment	
5	NorESM1-M	RCP8.5	Medium	No	Core experiments (Tier 1)	
6	MIROC-ESM-CHEM	RCP8.5	Medium	No		
7	NorESM1-M	RCP2.6	Medium	No		
8	CCSM4	RCP8.5	Medium	No		
9	NorESM1-M	RCP8.5	High	No		
10	NorESM1-M	RCP8.5	Low	No		
12	CCSM4	RCP8.5	Medium	Yes		
13	NorESM1-M	RCP8.5	PIGL-Medium	No		
A5	HadGEM2-ES	RCP8.5	Medium	No		Extended ensemble (Tier 2)
A6	CSIRO-Mk3.6.0	RCP8.5	Medium	No		
A7	IPSL-CM5A-MR	RCP8.5	Medium	No		
A8	IPSL-CM5A-MR	RCP2.6	Medium	No		
B6	CNRM-CM6-1	SSP5-8.5	Medium	No	CMIP6 extension (Tier 2)	
B7	CNRM-CM6-1	SSP1-2.6	Medium	No		
B8	UKESM1-0-LL	SSP5-8.5	Medium	No		
B9	CESM2	SSP5-8.5	Medium	No		
B10	CNRM-ESM2-1	SSP5-8.5	Medium	No		

**Table 2.** Extended ISMIP6-Antarctica Tier-1 and 2 future climate experiments for the period 2015–2300 discussed in this study. See Nowicki and others (2020) for references for the GCMs.



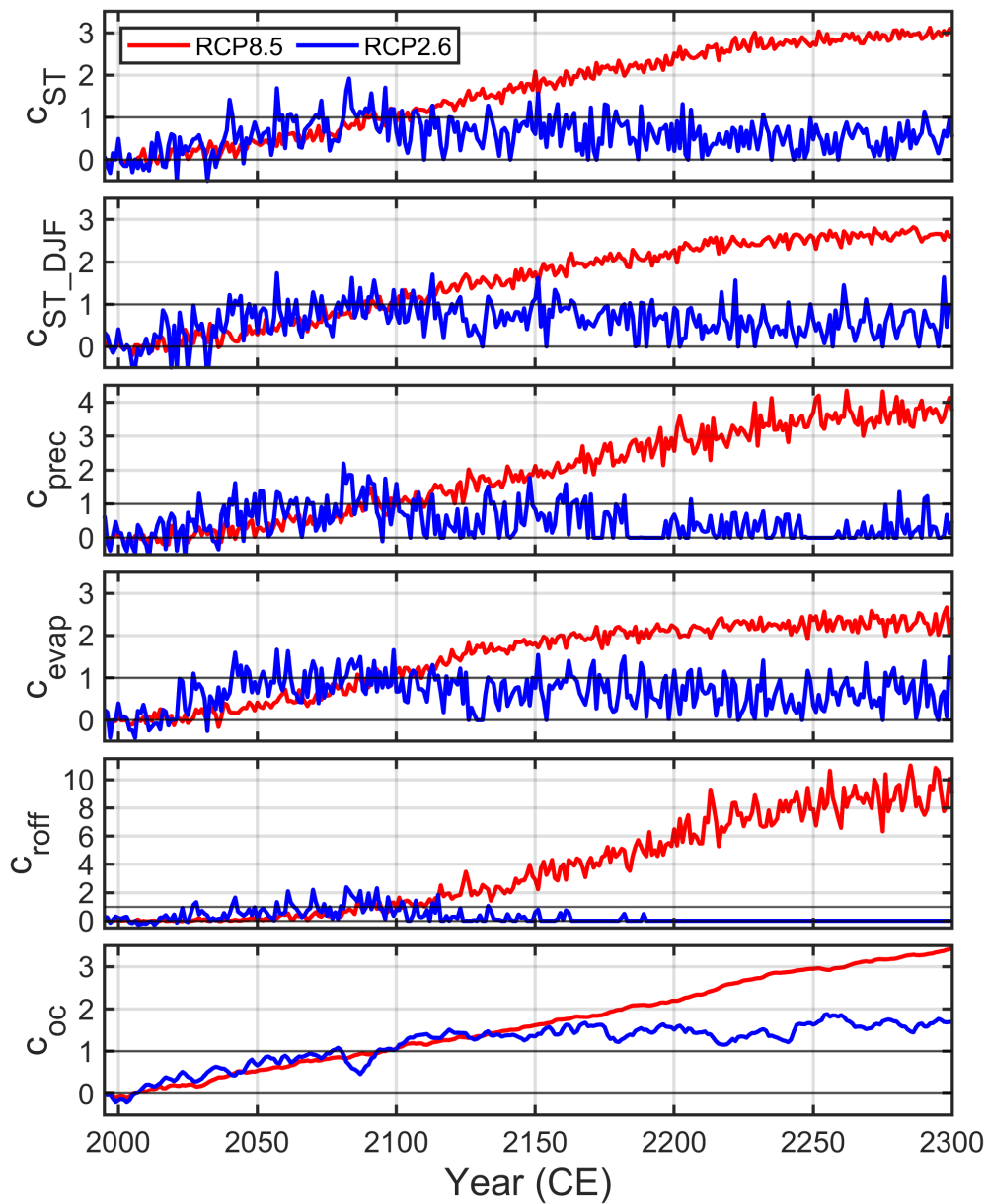


**Fig. 1.** RCP8.5 and RCP2.6 climate indices for the mean-annual surface temperature ( $c_{ST}$ ), DJF surface temperature ( $c_{ST\_DJF}$ ), precipitation ( $c_{prec}$ ), evaporation ( $c_{evap}$ ), surface runoff ( $c_{roff}$ ) and ocean temperature ( $c_{oc}$ ), derived from MIROC4m simulations until the year 2300. Note that the scaling defined by Eq. (1) implies that any non-zero value or variability of the indices corresponds to a stronger climate change for RCP8.5 than for RCP2.6.

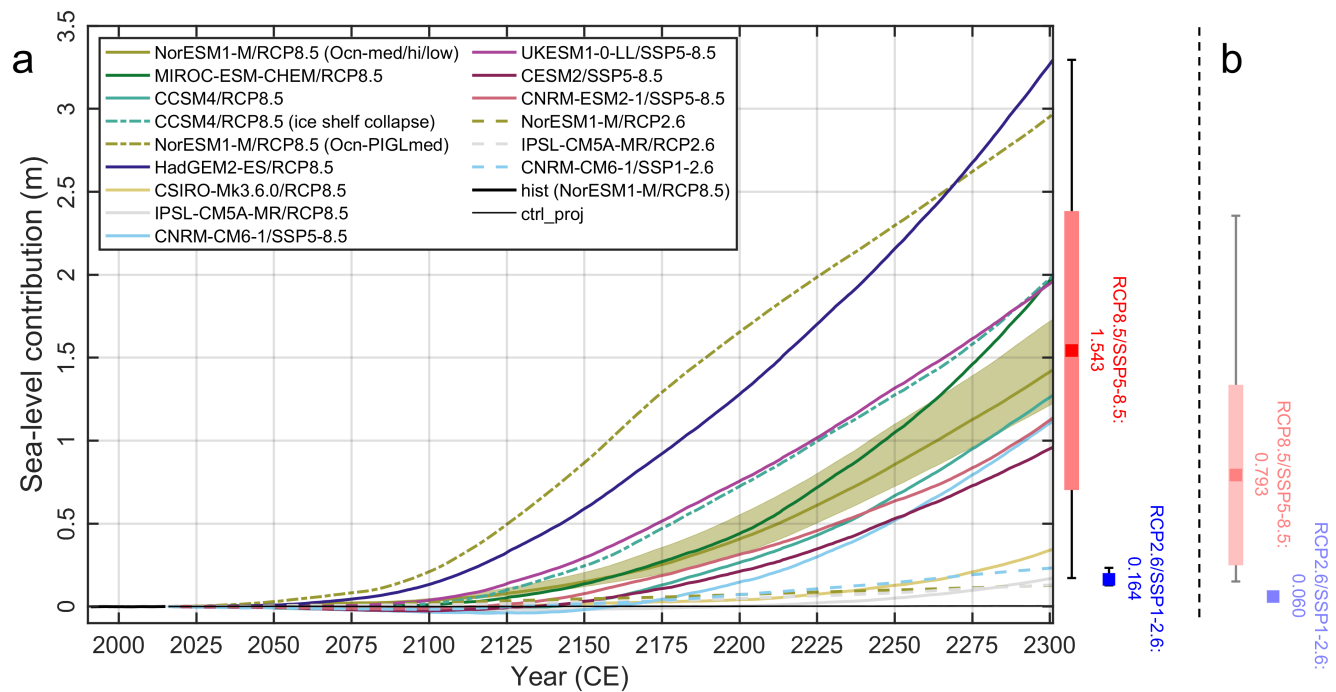


**Fig. 2.** (a) ISMIP6-Antarctica historical run (hist), projection control run (ctrl\_proj) and Tier-1 and 2 future climate experiments extended until 2300: Simulated ice mass change, counted positively for loss and expressed as a sea-level contribution. Experiments in the legend grouped such that RCP8.5/SSP5-8.5 comes first and RCP2.6/SSP1-2.6 thereafter, otherwise like in Table 2. The red and blue boxes to the right show the 2300 means for RCP8.5/SSP5-8.5 and RCP2.6/SSP1-2.6, respectively (RCP8.5/SSP5-8.5: also  $\pm 1$ -sigma); the whiskers show the corresponding full ranges. (b) Same 2300 statistics, but for the results by Chambers and others (2022) without a further warming trend beyond 2100.

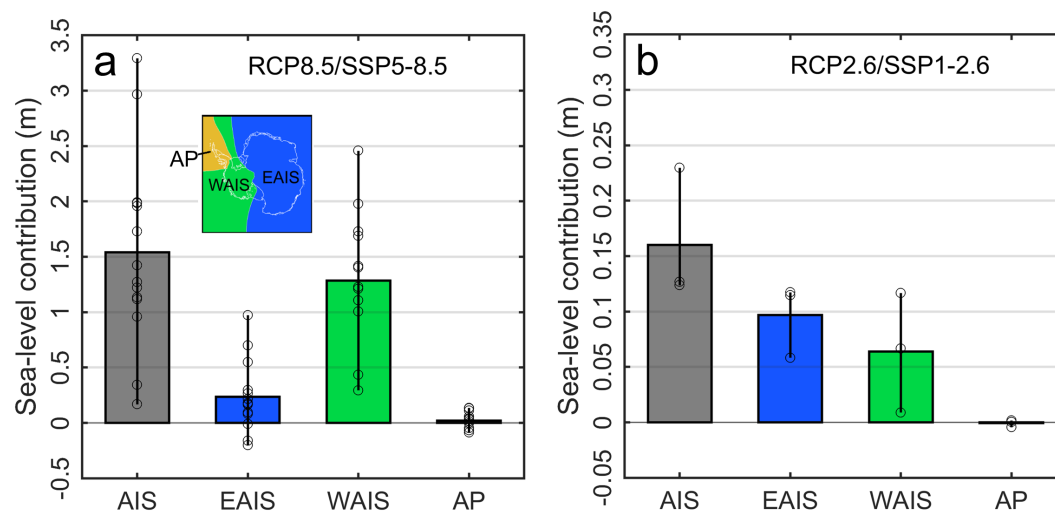


**Fig. 3.** Simulated sea-level contribution for the entire ice sheet and three regions (EAIS, WAIS, AP; shown in the inset) by the year 2300 relative to *ctrl\_proj*, for (a) the RCP8.5/SSP5-8.5 and (b) the RCP2.6/SSP1-2.6 ensemble. The whiskers show the full range of sea-level contributions across the simulations that make up the means, and the circles on the whiskers show the result for each simulation. Note that the  $y$ -axis ranges are different by a factor of 10.

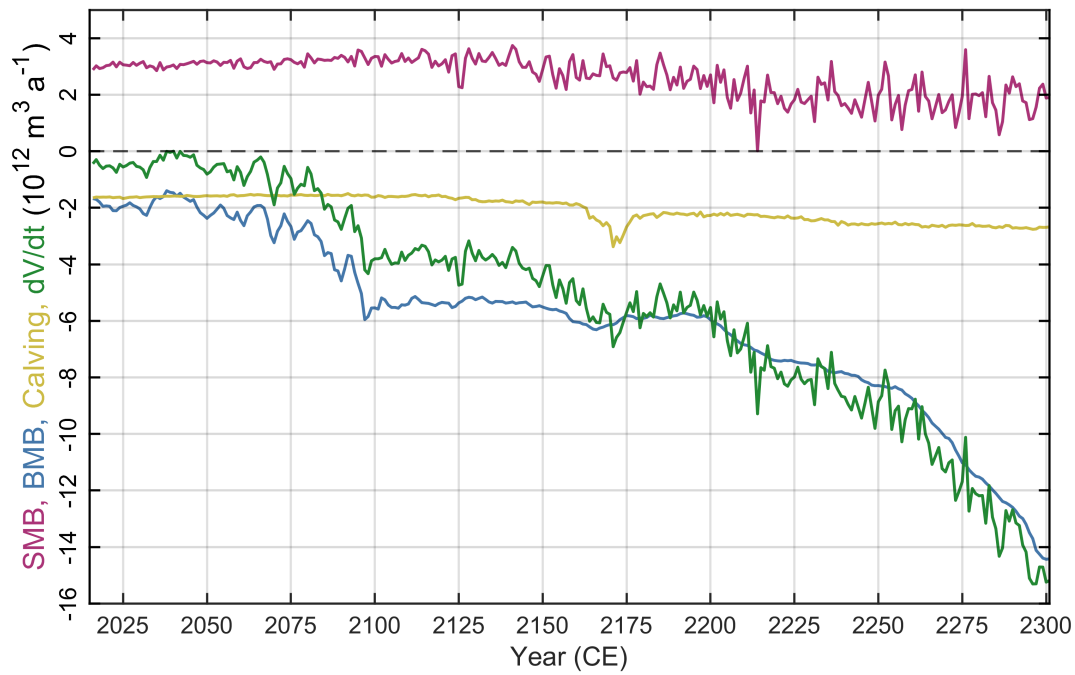


**Fig. 4.** Main components of the global mass balance for Exp. 6 (MIROC-ESM-CHEM/RCP8.5): Surface mass balance (SMB, purple), basal mass balance (BMB, blue), calving (yellow) and ice volume change ( $dV/dt$ , green).

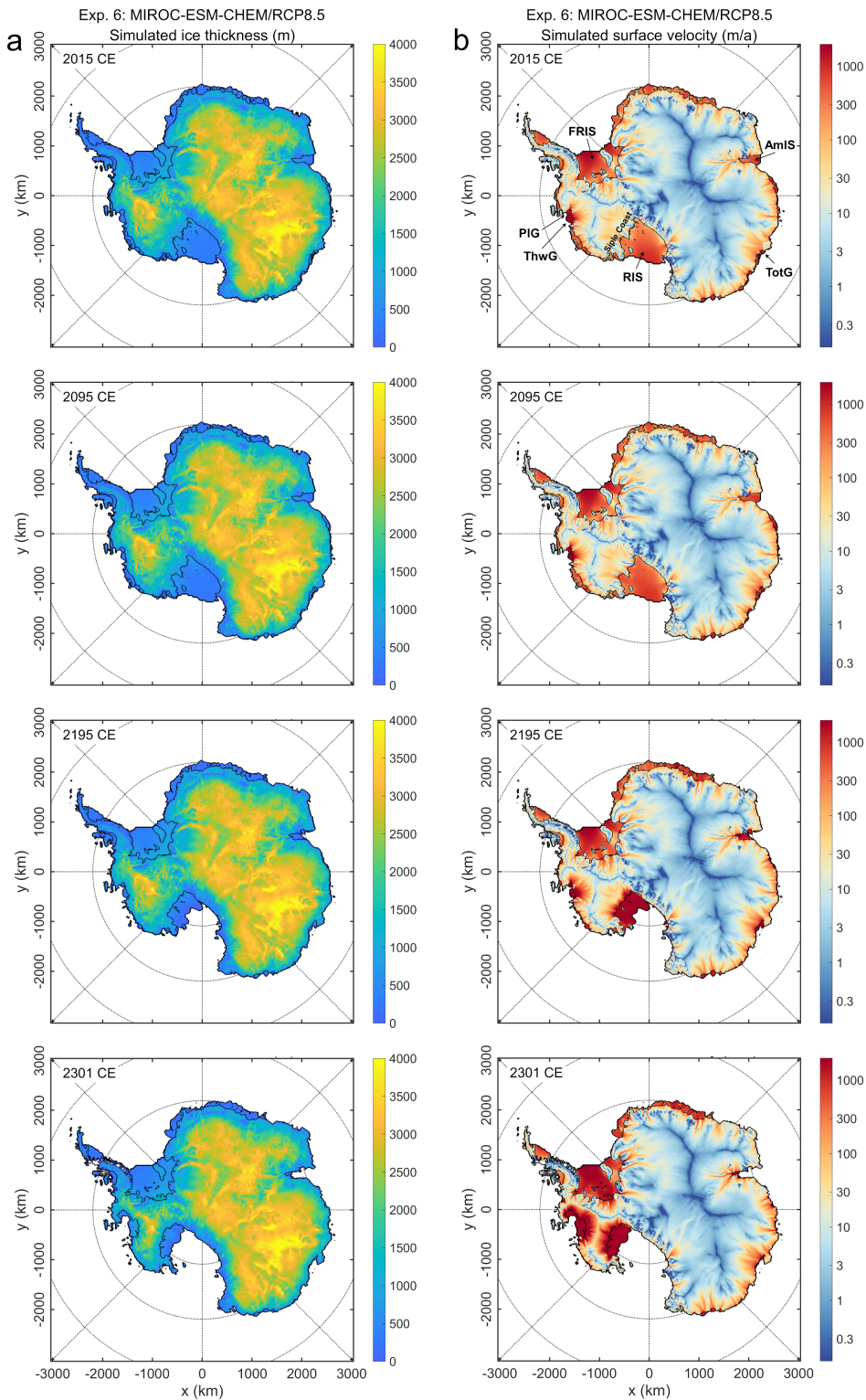


**Fig. 5.** Snapshots of (a) the simulated ice thickness and (b) the surface velocity for Exp. 6 (MIROC-ESM-CHEM/RCP8.5) for the years 2015, 2095, 2195 and 2301 (i.e., the end of 2300). Spacing of the latitude circles is  $10^\circ$ , spacing of the longitude rays is  $45^\circ$ . RIS: Ross Ice Shelf, FrIS: Filcher–Ronne Ice Shelf, AmIS: Amery Ice Shelf, PIG: Pine Island Glacier, ThwG: Thwaites Glacier, TotG: Totten Glacier.

540 **A ADDITIONAL GLOBAL MASS BALANCE ANALYSIS**

541 In addition to the discussion of the global mass balance for Exp. 6 (MIROC-ESM-CHEM/RCP8.5) pre-  
542 sented in Sect. 4, we carry out a similar analysis for Exps. 5 and 7 (NorESM1-M/RCP8.5, NorESM1-  
543 M/RCP2.6) to allow a direct comparison between an RCP8.5 and an RCP2.6 experiment (Fig. 6). By  
544 the end of 2300, Exp. 5 produces a mass loss of 1.43 m SLE, lower than that of Exp. 6 and slightly below  
545 the RCP8.5/SSP5-8.5 ensemble mean. The components of the global mass balance evolve generally in a  
546 similar way as for Exp. 6 (Fig. 4). The most notable difference is that SMB keeps on increasing over the  
547 entire model time. Further, both BMB and calving become less negative. All these factors work in the  
548 same direction and contribute to the smaller mass loss.

549 The mass loss produced by Exp. 7 by the end of 2300 is 0.127 m SLE. This is the smallest value of our  
550 three RCP2.6/SSP1-2.6 experiments (but almost equal to that of Exp. A8). In contrast to Exp. 5 where  
551 BMB dominates, BMB and calving contribute approximately the same to the mass loss until the end of  
552 the simulation. SMB is positive and almost constant. The residual between the mass gain from SMB and  
553 the losses from BMB and calving is negative, but small, which leads to a net mass loss less than 10% than  
554 that of Exp. 5.

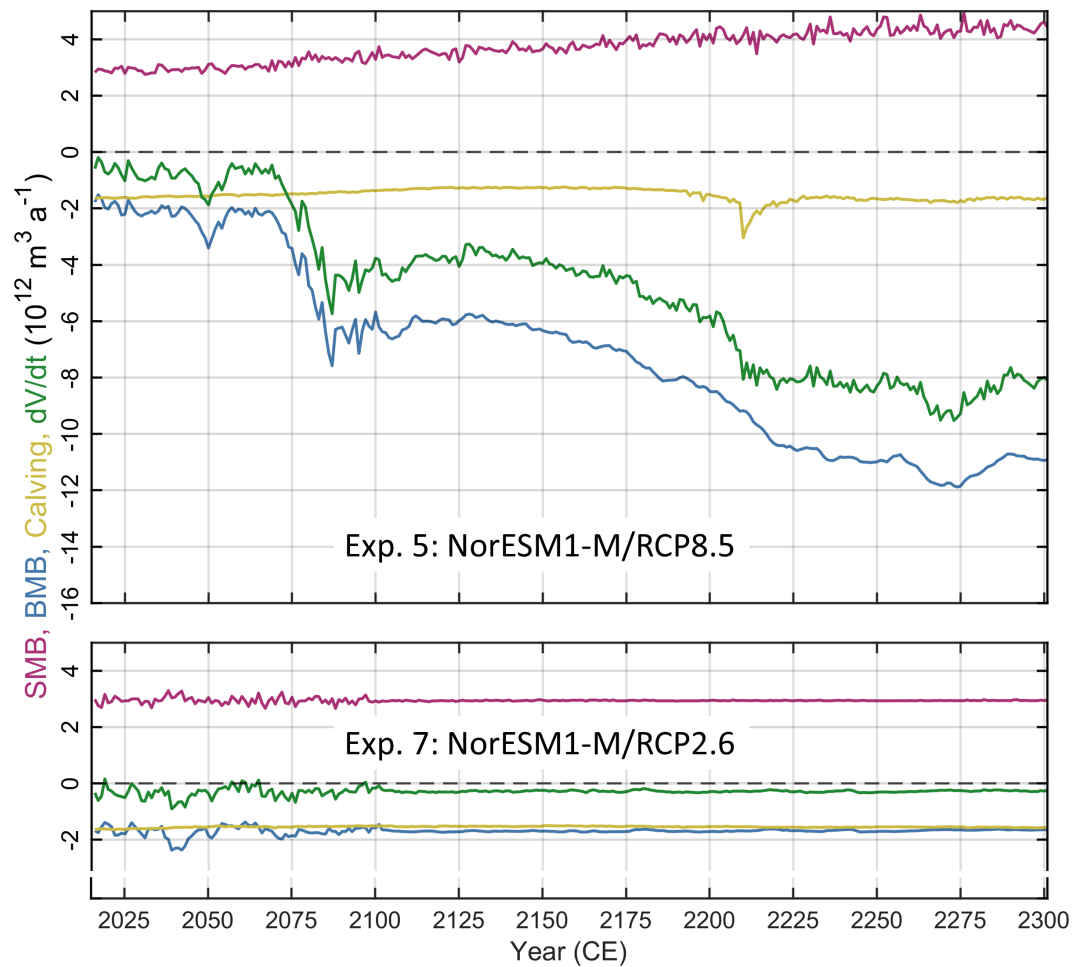


**Fig. 6.** Main components of the global mass balance for Exps. 5 and 7 (NorESM1-M/RCP8.5, NorESM1-M/RCP2.6): Surface mass balance (SMB, purple), basal mass balance (BMB, blue), calving (yellow) and ice volume change ( $dV/dt$ , green).